Chemical Science

Cite this: *Chem. Sci.*, 2012, **3**, 1137

www.rsc.org/chemicalscience

EDGE ARTICLE

Observation and investigation of the uranyl tetrafluoride dianion ($UO_2F_4^{2-}$) and its solvation complexes with water and acetonitrile†

Phuong Diem Dau,[a] Jing Su,[b] Hong-Tao Liu,[a] Jian-Biao Liu,[b] Dao-Ling Huang,[a] Jun Li*[b] and Lai-Sheng Wang*[a]

Received 11th December 2011, Accepted 23rd December 2011
DOI: 10.1039/c2sc01052f

Bare uranyl tetrafluoride ($UO_2F_4^{2-}$) and its solvation complexes by one and two water or acetonitrile molecules have been observed in the gas phase using electrospray ionization and investigated by photoelectron spectroscopy and *ab initio* calculations. The isolated $UO_2F_4^{2-}$ dianion is found to be electronically stable with an adiabatic electron binding energy of 1.10 ± 0.05 eV and a repulsive Coulomb barrier of ~2 eV. Photoelectron spectra of $UO_2F_4^{2-}$ display congested features due to detachment from U–O bonding orbitals and F 2p lone pairs. Solvated complexes by H_2O and CH_3CN, $UO_2F_4(H_2O)_n^{2-}$ and $UO_2F_4(CH_3CN)_n^{2-}$ (n = 1, 2), are also observed and their photoelectron spectra are similar to those of the bare $UO_2F_4^{2-}$ dianion, suggesting that the solvent molecules are coordinated to the outer sphere of $UO_2F_4^{2-}$ with relatively weak interactions between the solvent molecules and the dianion core. Both DFT and CCSD(T) calculations are performed on $UO_2F_4^{2-}$ and its solvated species to understand the electronic structure of the dianion core and solute–solvent interactions. The strong U–F interactions with partial (d–p)π bonding are shown to weaken the U=O bonds in the $[O{=}U{=}O]^{2+}$ unit. Each H atom in the water molecules forms a H-bond to a F atom in the equatorial plane of $UO_2F_4^{2-}$, while each CH_3CN molecule forms three H-bonds to two F ligands and one axial oxygen.

1. Introduction

Knowledge about the speciation and coordination chemistry of uranium compounds is essential in understanding the fate and transport of nuclear wastes, as well as recycling spent nuclear reactor fuels.[1] The uranyl dication (UO_2^{2+}) is known to be the most stable form of uranium in solution,[1–7] and it readily forms complexes with anionic ligands or solvent molecules. Exploring the chemical bonding of the uranyl ion with various ligands can help the elucidation of the metal–ligand binding and aid the development of efficient and selective ligands for the separation of fission products. Among stable uranyl species, much attention has been focused on the uranyl-halide complexes because they are particularly important in the extraction of uranium into the aqueous phase. The fluoride anion has a high charge density and a strong affinity for hard cations, such as UO_2^{2+}. Indeed, among uranyl-halide complexes, the U–F bonding in $UO_2F_n^{m-}$ is known to be the strongest in the condensed phases.[8–10] In the gas phase, the asymmetric vibrational frequency (ν_3) of the linear $[O{\equiv}U{\equiv}O]^{2+}$ unit in $UO_2F(acetone)_3^+$ is about 956 cm^{-1},[9] which is lower than that in the Cl, Br and I complexes. The fact that the $UO_2F_3^-$ anion cannot be measured with the infrared multi-photon dissociation experiments[9] supports the strong bonding in the uranyl fluoride complexes. In addition, the U–F bonding has been investigated using ligand exchange.[11–15] The exchange rate and the different coordination number of the uranyl fluoride have been found to affect its luminescence lifetimes.[16] Temperature-dependent studies in aqueous solution showed that coordination of fluoride to the uranyl dication is highly stable even at elevated temperatures.[17]

The coordination chemistry of $UO_2F_n^{m-}$ is still a subject of current interest. UO_2^{2+} is known to be able to accept up to five fluoride ligands, but $UO_2F_5^{3-}$ is unstable in solution due to ligand dissociation,[11,13] whereas $UO_2F_4^{2-}$ is very stable.[8] However, there have been no crystallographic reports on isolated $UO_2F_4^{2-}$ complexes, which always appear to contain a H_2O molecule as the fifth ligand.[18–20] In solution, results from extended X-ray absorption fine structure (EXAFS) also indicate that a solvent molecule, such as water or acetonitrile, can enter the first coordination sphere of $UO_2F_4^{2-}$.[8] Therefore, UO_2^{2+} tends to associate with a fifth solvent ligand in the condensed

[a]*Department of Chemistry, Brown University, Providence, RI, 02912, USA. E-mail: lai-sheng_wang@brown.edu*
[b]*Department of Chemistry & Key Laboratory of Organic Optoelectronics and Molecular Engineering of Ministry of Education, Tsinghua University, Beijing, 100084, China. E-mail: junli@mail.tsinghua.edu.cn*

† Electronic supplementary information (ESI) available: Photon-energy dependent spectra of $UO_2F_4(H_2O)_n^{2-}$ and $UO_2F_4(CH_3CN)_n^{2-}$ (n = 1, 2) and calculated vertical detachment energies and state energies of $UO_2F_4^{2-}$ at different levels of theory. See DOI: 10.1039/c2sc01052f

phases, in addition to the four fluoride anions. On the other hand, isolated $UO_2F_4^{2-}$ has been studied in numerous theoretical calculations,[8,21–28] though it has never been observed experimentally in the gas phase.

In the uranyl dication, the uranium atom forms two strong triple U≡O bonds with the oxygen atoms in a linear geometry ($D_{\infty h}$, $^1\Sigma_g^+$).[2–6] The frontier bonding molecular orbitals of UO_2^{2+} (σ_u, σ_g, π_g and π_u) are fully occupied by 12 valence electrons. The lowest unoccupied molecular orbitals (LUMOs) are the nonbonding uranium 5f-type orbitals, $5f\delta_u$ and $5f\phi_u$, because their symmetries are not suitable to mix with the occupied orbitals of UO_2^{2+}. Hence, there are ten frontier molecular orbitals (σ_u, σ_g, π_g, π_u, δ_u and ϕ_u) in UO_2^{2+} available to interact with the 2p orbitals of F^- in $UO_2F_4^{2-}$. The equatorial fluoride ligands primarily interact with the $5f\phi_u$ orbitals, with much weaker interaction with the $5f\delta_u$ orbitals,[6] whereas the orbital interaction and electrostatic repulsion from the F^- ligands can weaken the axial U–O bonding.[2–6] The fluoride anion bonds strongly to the uranyl dication in the condensed phases, but little is known about how the fluoride complexation would affect the U–O bonding in isolated uranyl-fluoride complexes. Despite numerous theoretical calculations on the uranyl complexes, there have been no experimental studies on the uranyl-fluoride species in the gas phase. Gas-phase experiments can provide direct information about chemical bonding in the uranyl-fluoride complexes and solute–solvent interactions.

Indeed, electrospray ionization (ESI) has been used previously for speciation of solutions and generation of gaseous uranyl complexes.[9,29–37] Spectroscopic studies have been carried out to probe the structures of various gaseous uranyl species.[9,38–41] We have developed an ESI photoelectron spectroscopy (PES) apparatus[42] to study multiply charged anions[43] and in general solution chemistry in the gas phase.[44] This technique is uniquely suitable to study negatively charged uranyl complexes, in particular, the uranyl-halide complexes. While multiply charged uranyl-halide anions have been investigated in the condensed phase,[8,10–13,15,17–20] no gas phase studies have been performed. Here, we report the first observation, in the gas phase, of the $UO_2F_4^{2-}$ dianion and its solvation complexes with one and two water or acetonitrile solvent molecules. PES experiments are carried out on the $UO_2F_4^{2-}$ dianion and its solvation complexes. We have found that $UO_2F_4^{2-}$ is electronically stable with an adiabatic electron binding energy (ADE) of 1.10 eV. The PES spectra of the solvated species are similar to the parent dianion with systematic solvation stabilization. Density function theory (DFT) and wavefunction-based *ab initio* calculations are performed to gain insight into the electronic structure of the $UO_2F_4^{2-}$ dianion and its solvation structures by one and two water or acetonitrile molecules. Our results show that the solvent molecules do not coordinate directly to the U atom in the first coordination sphere in $UO_2F_4^{2-}$ in the gas phase.

2. Experimental and theoretical methods

2.1. Electrospray and photoelectron spectroscopy

The experiment was carried out using our ESI-PES apparatus, which was described in detail previsouly.[42] The only modification was the shortening of the electron flight tube of the magnetic-bottle photoelectron analyzer from 4.5 to 2.5 m, leading to a slight decrease of electron energy resolution. Briefly, the anions, $UO_2F_4^{2-}$, $UO_2F_4(H_2O)_n^{2-}$ and $UO_2F_4(CH_3CN)_n^{2-}$ ($n = 1, 2$) were produced by electrospray of a 1 mM solution of $UO_2(CH_3CO_2)_2 \cdot 2H_2O$ in acetonitrile containing a trace amount of water. The fluoride complexes were formed by adding a small amount of AgF in the electrospray solution. A radio frequency-only quadrupole device guided the anions from the ESI source into a Paul trap operated at room temperature, where anions were accumulated for 0.1 s before being pulsed into the extraction zone of a time-of-flight mass spectrometer. Under our ESI condition, strong $UO_2F_4^{2-}$ dianion signals were produced. In addition, we also observed solvated complexes with one and two water or acetonitrile molecules. The desired anion was selected by a mass-gate and decelerated before being intercepted with a laser beam in the detachment region of the magnetic-bottle photoelectron analyzer. Three different lasers were used for the PES experiment. An F_2 excimer laser (157 nm, 7.866 eV) was used to probe a wide binding energy range. To enhance the spectral resolution, we performed PES experiments at lower photon energies, 213 nm (5.821 eV) from a dye laser, and 266 nm (4.661 eV) and 355 nm (3.496 eV) from a Nd:YAG laser. The PES spectra were calibrated using the known spectra of Au^- and I^-. The Au^- anion was produced by electrospray of a pyridine solution of AuCl with $NaSCH_3$ as the reducing agent. The electron kinetic energy resolution of the current magnetic-bottle photoelectron analyzer with the shortened electron flight tube was about 3%, *i.e.*, 30 meV for 1 eV electrons.

2.2. Theoretical and computational methods

The theoretical studies were carried out using both DFT and *ab initio* wavefunction theory (WFT) methods. DFT calculations were accomplished on $UO_2F_4^{2-}$, $UO_2F_4(H_2O)_n^{2-}$ and $UO_2F_4(CH_3CN)_n^{2-}$ ($n = 1, 2$) and their monoanions using the generalized gradient approximation (GGA) with the PBE exchange–correlation functional[45] implemented in the Amsterdam Density Functional (ADF 2010.01) program.[46–48] The Slater basis sets with the quality of triple-ζ plus two polarization functions (TZ2P)[49] were used, with the frozen core approximation applied to inner shells [$1s^2$–$5d^{10}$] for U, [$1s^2$] for O and F. The scalar relativistic (SR) and spin–orbit (SO) coupling effects were taken into account by the zero-order-regular approximation (ZORA).[50] Geometries were fully optimized at the SR-ZORA level and single-point energy calculations were performed with inclusion of the SO effects *via* the SO-ZORA approach.

To compare with the experiment, we performed *ab initio* WFT calculations for $UO_2F_4^{2-}$ using more advanced electron correlation methods in the MOLPRO 2008.1 program.[51] Both the CCSD(T) (coupled-cluster with single and double and perturbative triple excitations) and CASSCF (complete-active-space self-consistent field) methods were used in these calculations. The structure of $UO_2F_4^{2-}$ was optimized at the level of CCSD(T) with SR effects included. Single-point CCSD(T) energies of the ground and excited states of $UO_2F_4^-$ were calculated at the optimized geometries of $UO_2F_4^{2-}$, which accurately generated state-specific SR energies for all the states. The electron binding energies corresponding to one-electron transitions from the closed-shell ground state of $UO_2F_4^{2-}$ to the ground and excited

states of $UO_2F_4^-$ were obtained using the CASSCF/CCSD(T)/SO approach,[52–54] where the SO splittings were treated as a perturbation to the SR state energies and were calculated on the basis of CASSCF wavefunctions with the diagonal matrix elements replaced by the individual CCSD(T) state energies. The SO coupling was included by using a state-interacting method with SO pseudopotentials. We also used the CASSCF/CR-EOM-CCSD(T)/SO approach, where CR-EOM-CCSD(T)[55] energies derived from the EOM-CCSD energies with completely renormalized EOM-CCSD(T) corrections as implemented in NWChem 6.0 were used as the diagonal elements.[56] In this approach, we used SR-ECP for CR-EOM-CCSD(T) calculations of the non-SOC state energies, while the SOC effects were included through the subsequent CASSCF/CR-EOM-CCSD(T)/SO calculations. The CR-EOM-CCSD(T) calculation was performed on the monoanion at the optimized CCSD(T) geometry of the dianion to obtain the energies of the excited states, with the CCSD(T) energy of the first state used as reference. In the MOLPRO and NWChem calculations, we used the Stuttgart energy-consistent relativistic pseudopotentials ECP60MWB (U)[57,58] and the corresponding valence triple-ζ basis sets aug-cc-pVTZ for O and F.[59]

3. Experimental results

3.1. Photoelectron spectroscopy of $UO_2F_4^{2-}$

Fig. 1 displays the photoelectron spectra of $UO_2F_4^{2-}$ at four different photon energies, 355, 266, 213 and 157 nm. The 157 nm spectrum (Fig. 1d) reveals many detachment features between 1 and 6 eV binding energies, which are labeled with letters (X, A–E). These features are all fairly broad owing to either large geometry changes from the dianion to the monoanion states and/or overlapping detachment channels. Thus, the spectral features are labeled for the sake of discussion and cannot be viewed as representing individual electronic transitions necessarily. At 213 nm (Fig. 1c), the bands D and E are cut off and the intensity of band C is significantly reduced due to the repulsive Coulomb barrier (RCB) expected for a dianion.[43] The spikes above 5 eV in the 213 nm spectrum are due to noise as a result of imperfect background subtraction. The cutoff of the higher binding energy features at 213 nm gives an estimate of the magnitude of the RCB ($h\nu$ – cutoff). Because of electron tunneling,[60] the RCB cannot define a sharp cutoff threshold and its height can only be estimated from the PES spectra at different photon energies. The 213 nm spectrum yields a RCB of about 2.0 eV, assuming the cutoff energy at about 4.0 eV.

At 266 nm (Fig. 1b), bands B and C are cut off subsequently, consistent with the 2.0 eV RCB estimated from the 213 nm spectrum. The sharp peak at 3.4 eV in the 266 nm spectrum is due to detachment of F^-, originated from photodissociation of the $UO_2F_4^{2-}$ parent at 266 nm ($UO_2F_4^{2-} \rightarrow UO_2F_3^- + F^-$). The electron binding energy of the $UO_2F_3^-$ fragment is too high for its photodetachment to be observed at 266 nm.[61] Similar photodissociation is also observed at 355 nm (Fig. 1a), as shown by the observation of the F^- detachment signal. At 355 nm, only the ground-state band X is observed and its higher binding energy side appears to be cut off, consistent with the estimated RCB height of 2.0 eV. The 355 nm spectrum is the best-resolved

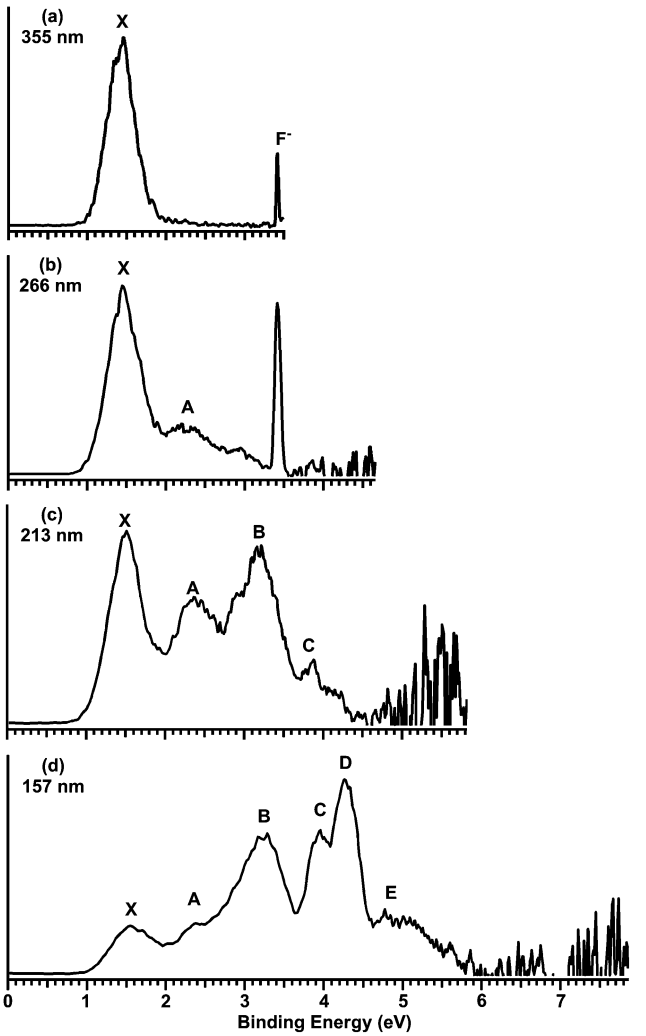

Fig. 1 Photoelectron spectra of $UO_2F_4^{2-}$ at (a) 355 nm (3.496 eV), (b) 266 nm (4.661 eV), (c) 213 nm (5.821 eV) and (d) 157 nm (7.866 eV).

spectrum and the detachment threshold yields an ADE of 1.10 ± 0.05 eV and a VDE of 1.46 ± 0.05 eV for the X band. The large ADE value indicates that $UO_2F_4^{2-}$ is highly electronically stable against electron loss, despite the strong intramolecular Coulomb repulsion in the doubly charged anion. The X band represents the detachment transition from the ground state of the $UO_2F_4^{2-}$ dianion to that of the $UO_2F_4^-$ monoanion. Thus, the ADE of

Table 1 Calculated and observed adiabatic detachment energy (ADE) and vertical detachment energy (VDE) of the first detachment band from the photoelectron spectra of $UO_2F_4^{2-}$

		CCSD(T)		DFT/PBE	
	Exptl.[a]	SR	SO[b]	SR	SO
ADE/eV	1.10(5)	1.36	1.20	0.18	0.02
VDE/eV	1.46(5)	1.84	1.72	0.47	0.35

[a] Numbers in parentheses represent the experimental uncertainties in the last digit. [b] These SO results are estimated using the SR CCSD(T) energies with the *ad-hoc* SO-corrections from DFT/PBE calculations.

1.10 eV is also the first electron affinity of the $UO_2F_4^-$ monoanion and the second electron affinity of neutral UO_2F_4 species. The ADE and VDE of $UO_2F_4^{2-}$ are compared with theoretical results in Table 1 at several levels of theory.

3.2. Photoelectron spectroscopy of $UO_2F_4(H_2O)_n^{2-}$ (n = 1, 2)

The photoelectron spectra of $UO_2F_4(H_2O)_n^{2-}$ (n = 1, 2) at 157 nm are shown in Fig. 2, in comparison with that of $UO_2F_4^{2-}$. We have also obtained data at 266 and 213 nm for the two H_2O-solvated complexes, which are given in Fig. S1 and S2 for n = 1 and 2, respectively, in the supplementary information (ESI†). The PES spectra of the two hydrated species are similar to that of the solute $UO_2F_4^{2-}$ dianion, except a systematic blue shift of the electron binding energies due to the solvation effects. The VDE for the first detachment band X is increased by about 0.5 eV per H_2O molecule. The estimated first ADE and VDE for $UO_2F_4(H_2O)_n^{2-}$ (n = 1, 2) are given in Table 2. At 266 nm, a sharp peak, which is labeled as the detachment of F^-, is also observed due to photodissociation of the solvated complexes (Figs. S1 and S2, ESI†), similar to that observed for the solute $UO_2F_4^{2-}$ at the same detachment laser wavelength (Fig. 1b). On the basis of the spectral cutoffs at 213 and 266 nm (Figs. S1 and S2, ESI†), we observed that the RCB in the hydrated complexes is also smaller, reduced to ~1.7 eV relative to ~2.0 eV in $UO_2F_4^{2-}$. The smaller RCB indicates decreased intramolecular Coulomb repulsion in the hydrated complexes, suggesting a small amount of charge delocalization from the solute dianion to the solvent. This observation, along with the similarity between the PES spectra of the hydrated complexes and that of the solute dianion, suggests that the H_2O molecules only coordinate to either F or O on the outside of the $UO_2F_4^{2-}$ dianion.

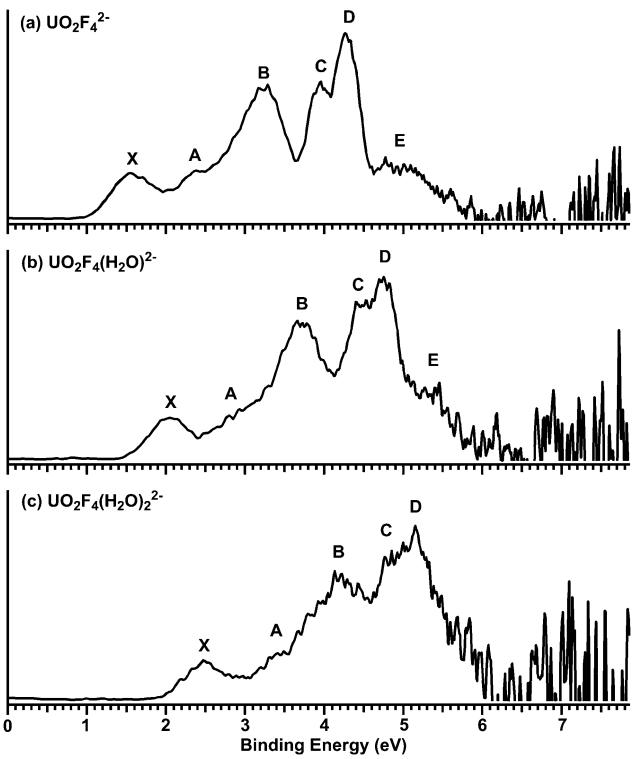

Fig. 2 Photoelectron spectra of (a) $UO_2F_4^{2-}$ in comparison with (b) $UO_2F_4(H_2O)^{2-}$ and (c) $UO_2F_4(H_2O)_2^{2-}$ at 157 nm.

3.3. $UO_2F_4(CH_3CN)_n^{2-}$ (n = 1, 2)

The photoelectron spectra of $UO_2F_4(CH_3CN)_n^{2-}$ (n = 1, 2) are compared with that of $UO_2F_4^{2-}$ in Fig. 3 at 157 nm. We also measured the PES spectra of the CH_3CN complexes at 266 and 213 nm, which are given in Fig. S3 and S4 for n = 1 and 2, respectively (ESI†). Again the PES spectra of the CH_3CN solvated species are similar to that of the solute dianion. The effects of the CH_3CN solvent on the $UO_2F_4^{2-}$ dianion are very similar to those of H_2O, except that CH_3CN provides a stronger stabilization effect. On average, each CH_3CN molecule increases the electron binding energies by almost 0.6 eV relative to that of the $UO_2F_4^{2-}$ dianion, as shown in Table 2, suggesting slightly stronger interactions between CH_3CN and $UO_2F_4^{2-}$.

4. Theoretical results

4.1. $UO_2F_4^{2-}$

The calculated first ADE and VDE for $UO_2F_4^{2-}$ at DFT/PBE and CCSD(T) levels of theory are compared with the experimental data in Table 1. The DFT/PBE methods significantly underestimate the electron binding energies for the dianion by about 1 eV, which has been observed in other dianions as well.[62] Inasmuch as the monoanion has an open-shell configuration that undergoes first-order SO splitting, while the dianion is closed-shell that does not have the first-order SO splitting, the calculated ADEs and VDEs are much larger for the SR formalism than for the SO one.[63] At DFT/PBE level, the calculated SO effects for the ADE and VDE of $UO_2F_4^{2-}$ are 0.16 and 0.12 eV, respectively (Table 1). The calculated SR CCSD(T) ADE and VDE values are already in better agreement with the experiment. Using the SO corrections from the PBE calculations and the SR CCSD(T) results, we estimate the ADE and VDE of $UO_2F_4^{2-}$ to be around 1.20 and 1.72 eV, respectively, which are still a little too high relative to the experiment. Table 3 displays the optimized bond lengths of U–O and U–F in both $UO_2F_4^{2-}$ and $UO_2F_4^-$. Upon electron detachment from $UO_2F_4^{2-}$, both DFT and CCSD(T) calculations show that the U–F bond lengths decrease in the $UO_2F_4^-$ monoanion, as a result of the reduced intramolecular Coulomb repulsion. The two methods give different trends for the U–O bond lengths between the dianion and monoanion, although both methods show that the U–O bond lengths change very slightly. It appears that DFT overestimates the effect of the intramolecular Coulomb repulsion on the U–O bond lengths in the dianion.

The occupied valence MO levels for $UO_2F_4^{2-}$ are shown in Fig. 4 with SR and SO effects included while details of the calculated VDEs for all the MOs by DFT/PBE can be found in Table S1 (ESI†). The top five MOs involve the σ and π bonding of $[O\equiv U\equiv O]^{2+}$, where the $3e_u$ orbitals display strong SO effects (Fig. 4) due to a small contribution of U 6p orbitals, as shown previously in UF_6 and UO_6.[64] The occupied molecular orbitals for $UO_2F_4^{2-}$ from DFT calculations are presented in Fig. 5. Clearly, the $2a_{2u}$, $2e_g$, $3e_u$ and $2a_{1g}$ are the U–O bonding orbitals and the remainder are primarily F 2p type orbitals that are virtually not affected by SO effects (Fig. 4).

Table 2 Observed and calculated adiabatic (ADE) and vertical (VDE) detachment energies for solvated uranyl tetrafluoride complexes in comparison with theoretical calculations

	Exptl.[a]/eV		Theor.[b]/eV			
			Est. CCSD(T)		SR-DFT/PBE	
	ADE	VDE	ADE^{SO}	VDE^{SO}	ADE^{SR}	VDE^{SR}
$UO_2F_4^{2-}$	1.10(5)	1.46(5)	1.20	1.72	0.18	0.47
$UO_2F_4(H_2O)^{2-}$	1.54(5)	1.95(5)	1.73	2.19	0.71	0.94
$UO_2F_4(H_2O)_2^{2-}$	2.03(5)	2.40(5)	2.20	2.60	1.18	1.35
$UO_2F_4(CH_3CN)^{2-}$	1.62(5)	2.02(5)	1.86	2.41	0.84	1.16
$UO_2F_4(CH_3CN)_2^{2-}$	2.15(5)	2.55(5)	2.44	3.00	1.42	1.75

[a] The numbers in parentheses represent the experimental uncertainties in the last digit. [b] The SR energies are calculated at the SR-DFT/PBE level of theory. The SO energies are corrected using the differential SO-correction for CCSD(T) energies from Table 1.

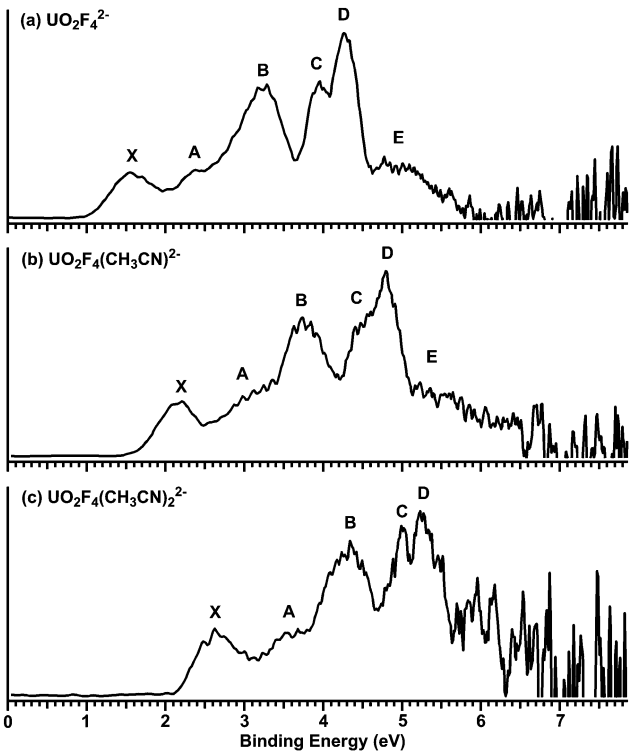

Fig. 3 Photoelectron spectra of (a) $UO_2F_4^{2-}$ in comparison with (b) $UO_2F_4(CH_3CN)^{2-}$ and (c) $UO_2F_4(CH_3CN)_2^{2-}$ at 157 nm.

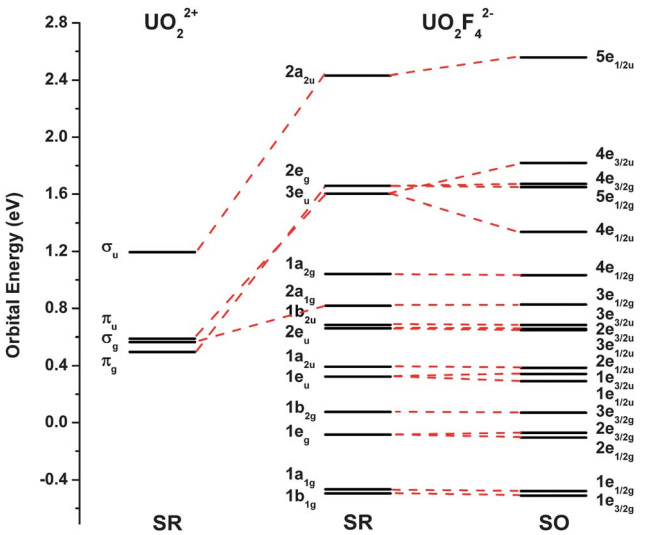

Fig. 4 The SR and SO energy levels of the frontier occupied orbitals of $UO_2F_4^{2-}$ calculated at DFT/PBE level. The $2a_{2u}$, $2e_g$, $3e_u$ and $2a_{1g}$ orbitals correspond to U–O bonding orbitals in UO_2^{2+} and all other orbitals are F 2p lone pairs.

Table 3 Optimized geometrical parameters for $UO_2F_4^{2-}$ and $UO_2F_4^{-}$

	Sym.	Method	U–O/Å	U–F/Å
$UO_2F_4^{2-}$	D_{4h}	DFT/PBE	1.8510	2.2333
$UO_2F_4^{-}$	D_{4h}	DFT/PBE	1.8499	2.1311
$UO_2F_4^{2-}$	D_{4h}	CCSD(T)	1.8082	2.2319
$UO_2F_4^{-}$	D_{4h}	CCSD(T)	1.8267	2.1092

Fig. 6 displays the simulated PES spectra of $UO_2F_4^{2-}$ by CR-EOM-CCSD(T) and CCSD(T) calculations. The simulated spectra are generally consistent with the experimental results qualitatively, especially the CR-EOM-CCSD(T) results (Fig. 6a) due to the partial inclusion of multi-reference treatment for excited states. The completed results of CCSD(T) and CR-EOM-CCSD(T) calculations were summarized in Table S2 (ESI†).

4.2. $UO_2F_4(H_2O)_n^{2-}$ (n = 1, 2)

For the hydrated $UO_2F_4^{2-}$ complexes, we carefully investigated various structures, including the cases in which water binds directly to uranyl. We found that the most stable structure is the one as shown Fig. 7a, in which water binds to the equatorial F ligands on the outer sphere and forms two H-bonds in a bidentate fashion. The optimized structure of $UO_2F_4(H_2O)_2^{2-}$ is shown in Fig. 7b. The second water molecule binds in exactly the same manner as the first water, forming two H-bonds with the two remaining F ligands. To see how the hydration may change the electronic structure of the solute $UO_2F_4^{2-}$, we simulated the PES spectra $UO_2F_4(H_2O)_n^{2-}$ (n = 1, 2) at the DFT level and compared with the simulated spectrum of $UO_2F_4^{2-}$ at the same level of theory in Fig. 8. As expected, the simulated PES spectra of the hydrated $UO_2F_4^{2-}$ complexes are

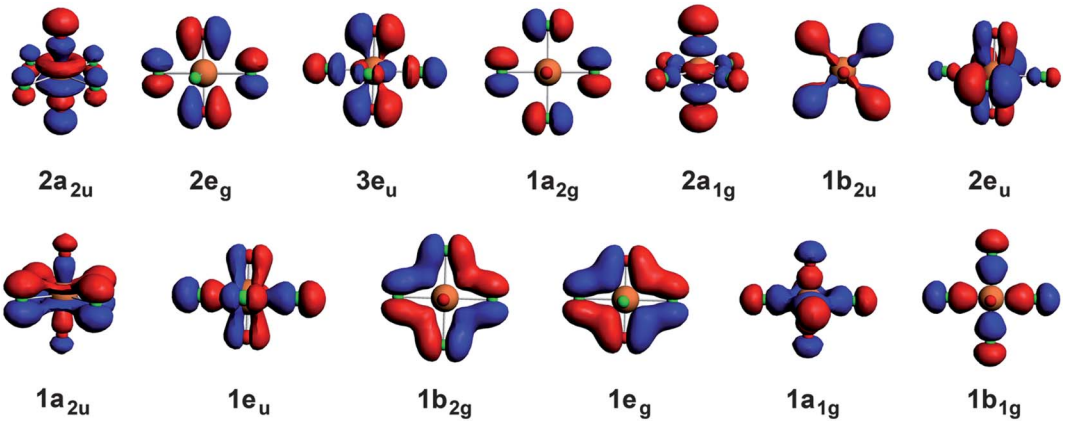

Fig. 5 The contour diagrams of the occupied valence orbitals of $UO_2F_4^{2-}$ at DFT/PBE level. The $2a_{2u}$ orbital is the HOMO.

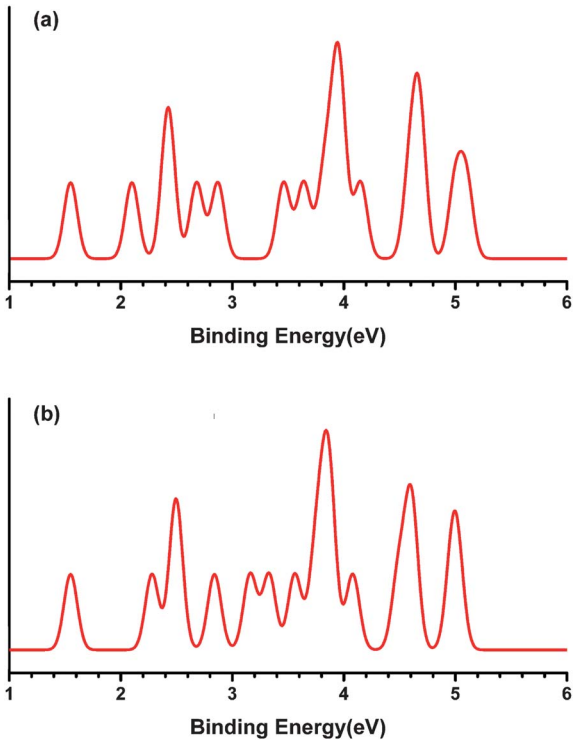

Fig. 6 Simulated photoelectron spectra of $UO_2F_4^{2-}$ from (a) CR-EOM-CCSD(T) and (b) CCSD(T) calculations. The simulated spectra were generated by fitting a Gaussian of 0.06 eV width to each calculated VDE.

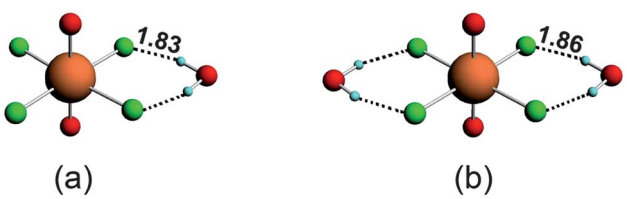

Fig. 7 Optimized structures of (a) $UO_2F_4(H_2O)^{2-}$ (C_{2v}) and (b) $UO_2F_4(H_2O)_2^{2-}$ (D_{2d}) at DFT/PBE level. The H-bond lengths are in Å.

nearly identical to the bare dianion, because the water molecules do not perturb the solute significantly by simply forming outer-sphere complexes.

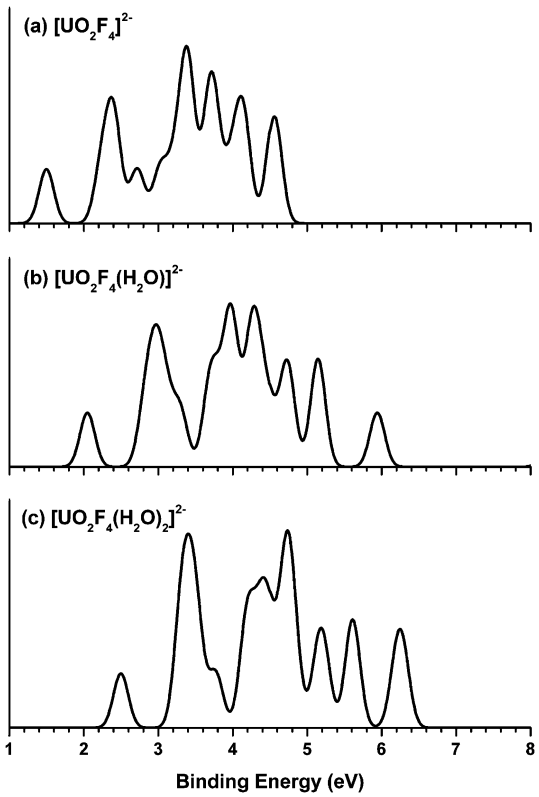

Fig. 8 Simulated photoelectron spectra of (a) $[UO_2F_4]^{2-}$, (b) $[UO_2F_4(H_2O)]^{2-}$ and (c) $[UO_2F_4(H_2O)_2]^{2-}$ from DFT/PBE calculations. See caption of Fig. 6.

4.3. $UO_2F_4(CH_3CN)_n^{2-}$ (n = 1, 2)

For the solvation complexes of $UO_2F_4^{2-}$ with acetonitrile, we also investigated different configurations, including coordination of CH_3CN directly to U *via* the N atom equatorially. We found that the most stable structures of $UO_2F_4(CH_3CN)_n^{2-}$ (n = 1, 2) are again outer-sphere complexes, as shown in Fig. 9. Surprisingly, our results show that the three H atoms in CH_3CN are all capable of forming H-bonds with $UO_2F_4^{2-}$: two with the equatorial F atoms and one with the axial O atom. This binding mode provides the maximal stabilization to the $UO_2F_4^{2-}$ dianion,

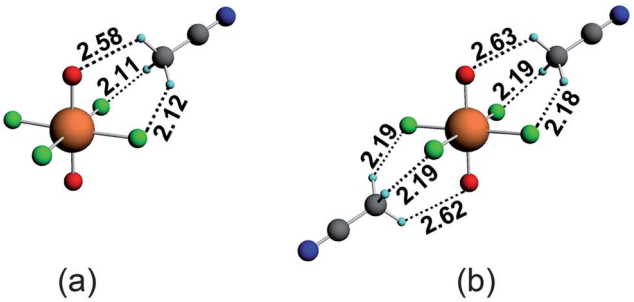

Fig. 9 Optimized structures of (a) $UO_2F_4(CH_3CN)^{2-}$ (C_1) and (b) $UO_2F_4(CH_3CN)_2^{2-}$ (C_1) at DFT/PBE level. The H-bond lengths are in Å.

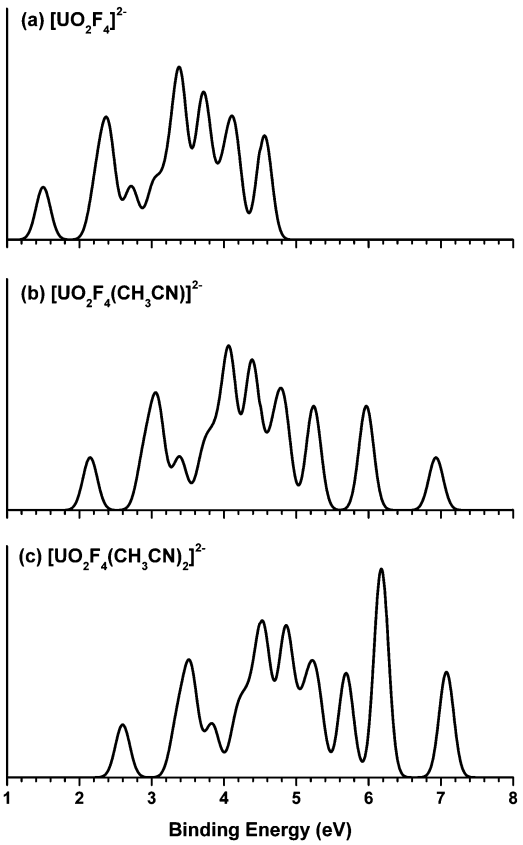

Fig. 10 Simulated photoelectron spectra of (a) $[UO_2F_4]^{2-}$, (b) $UO_2F_4(CH_3CN)^{2-}$ and (c) $UO_2F_4(CH_3CN)_2^{2-}$ from DFT/PBE calculations. See caption of Fig. 6.

consistent with the experimental observation that the electron binding energies of the CH_3CN-solvated species are higher than the hydrated complexes. The simulated PES spectra of $UO_2F_4(CH_3CN)_n^{2-}$ ($n = 1, 2$) at DFT level are compared with that of $UO_2F_4^{2-}$ in Fig. 10, showing that the outer-sphere CH_3CN solvents have very little perturbation to the electronic structure of the bare dianion.

5. Discussions

5.1. $UO_2F_4^{2-}$

Fig. 4 and 5 show that the HOMO ($2a_{2u}$) of $UO_2F_4^{2-}$ is mainly the σ_u orbital of UO_2^{2+}. Detachment from the HOMO gives rise to the X band in the PES spectra (Fig. 1), corresponding to the ground state of the monoanion $UO_2F_4^-$. The X band is well separated from the A band in agreement with the MO diagram in Fig. 4, where the HOMO is shown to be well spaced from the deeper MOs. The broad spectral width of the X band suggests a large geometry relaxation between the ground state of $UO_2F_4^{2-}$ and that of the monoanion $UO_2F_4^-$. This observation is also borne out from our theoretical calculations, as shown in Table 3. We note that the calculated U–O and U–F bond lengths in $UO_2F_4^{2-}$ are consistent with previous calculations at B3LYP and MP2 levels.[8a] Both DFT and CCSD(T) results show that the U–F bonds are shortened by 0.1 Å in the monoanion, while the U–O bonds do not change significantly. The ADE of the X band is measured to be 1.10 eV, suggesting that the $UO_2F_4^{2-}$ dianion is a highly electronically stable gaseous dianion despite the large intramolecular Coulomb repulsion. As shown in Table 1, DFT calculations significantly underestimate the electronic stability of the $UO_2F_4^{2-}$ dianion by about 1 eV. The CCSD(T) calculations give better estimation of ADE (1.20 eV) and VDE (1.72 eV) for $UO_2F_4^{2-}$, compared to the experimental values of 1.10 and 1.46 eV, respectively.

According to the MO diagram in Fig. 4, the broad band A should come from detachments from the $2e_g$ and $3e_u$ orbitals, which are primarily the π_g and π_u bonding orbitals of the UO_2^{2+} uranyl unit. SO coupling has little effect on the $2e_g$ MOs because of the small SO splitting of U 6d (*gerade*), but it leads to considerable splitting of the $3e_u$ MOs due to the large differential SO effect of U 5f (*ungerade*), thus giving rise to the broad A band. As shown in Fig. 4, the remaining MOs are mainly of F 2p character (except $2a_{1g}$), which are closely spaced. The high density of electronic states plus the expected geometry relaxation upon electron detachment gives rise to the congested PES spectra for $UO_2F_4^{2-}$. The simulated spectra in Fig. 6 at both CR-EOM-CCSD(T) and CCSD(T) levels are in qualitative agreement with the experimental spectra. Applications of similar CASSCF/CCSD(T)/SO approach to the $UO_2Cl_2(Ar)_n$ and UF_6 molecules have yielded highly accurate energies for their excited states,[65,66] validating the accuracy of such approach for actinide excited states.

As shown in Table 3, both DFT and CCSD(T) calculations show that the U–F bond lengths in $UO_2F_4^{2-}$ are about 2.23 Å. The U–F bond lengths are reduced by ~0.1 Å in the monoanion $UO_2F_4^-$, largely due to the reduced intramolecular Coulomb repulsion. CCSD(T) predicts a slightly shorter U–O bond length (1.83 Å) in $UO_2F_4^{2-}$ than that predicted by DFT (1.85 Å). Both are longer than the U–O bond length in neutral uranyl complexes[66,67] and the condensed phase: 1.800 Å in solution[8] and 1.780 Å in solid state,[19] although in the condensed phases $UO_2F_4^{2-}$ possesses a fifth water molecule ligand in the equatorial position.[8,18–20] Both DFT and CCSD(T) calculations (Table 2) show that the U–O bond lengths do not change significantly upon electron detachment from $UO_2F_4^{2-}$. However, the CCSD(T) results given in Table 3 correctly capture the elongation of the U–O bond upon detachment of one electron from the U–O bonding σ_u orbital, whereas DFT overestimates the effect on U–O distance from the decrease of Coulomb repulsion of the overall dianion. As shown in Fig. 5, the HOMO of $UO_2F_4^{2-}$ is mainly a σ_u bonding orbital and the U–O bond length is expected to increase in the $UO_2F_4^-$ monoanion.

The apparent insensitivity of the U–O bond lengths to charge states is likely due to the balance between intramolecular Coulomb repulsion in the dianion and U–O chemical bonding. In the dianion, the strong intramolecular Coulomb repulsion is expected to stretch the U–O bond. Therefore, the release of the Coulomb repulsion in the monoanion (shortening the U–O bonds) balances the effects due to the removal of a bonding electron (lengthening the U–O bonds). The DFT method probably overestimates the electrostatic repulsion in the dianion, leading to an overestimated U–O bond length and much too low ADE and VDE as compared to the CCSD(T) results. Indeed, the U–O bonds in the penta-coordinated $UO_2F_4(H_2O)^{2-}$ are measured to be 1.80 Å in solution from EXAFS.[8b] The shorter U–O bond lengths in solution than in isolated $UO_2F_4^{2-}$ are understandable due to the solvent shielding of the intramolecular Coulomb repulsion. There has been much interest about the level of participation of the 5f orbitals in the U–O bonding.[2–6] The HOMO depicted in Fig. 5 for $UO_2F_4^{2-}$ shows clear contribution of the 5fσ orbital in agreement with previous works. In addition, the $3e_u$ orbital (HOMO−2) reveals significant 5f π character.

5.2. $UO_2F_4(H_2O)_n^{2-}$ ($n = 1, 2$)

The PES spectra of $UO_2F_4^{2-}$ solvated with one and two water molecules (Fig. 2) are nearly identical to that of the bare dianion except for the blue shifts toward higher binding energies. Each water molecule is observed to provide roughly the same stabilization by ~0.5 eV to the electron binding energy relative to the bare dianion. These observations suggest that the water molecules do not perturb the electronic structure of $UO_2F_4^{2-}$ significantly and are likely interacting with the dianion on the outer sphere, as borne out from our theoretical calculations (Fig. 7). Each water molecule forms two H-bonds with the equatorial F ligands. This bonding mode is also consistent with the fact that we did not observe $UO_2F_4^{2-}$ solvated with three water molecules. The first two waters form a strong first solvation shell and the third water is expected to be more weakly bonded. The simulated PES spectra for $UO_2F_4(H_2O)_n^{2-}$ (Fig. 8) are similar to that of the bare dianion, providing further evidence for the outer-sphere solvation structure.

Our observation of the solvation structures of $UO_2F_4^{2-}$ by water is consistent with previous computational studies for gas-phase $UO_2F_4^{2-}$.[22,24,25,27,28] However, in the condensed phase, $UO_2F_4^{2-}$ is known to prefer penta-coordination in the equatorial plane with one water molecule directly coordinated to the U atom. It has been shown that solvent effects and the presence of counter ions in the condensed phases are important to stabilize the penta-coordination.[24] Indeed, the equatorial penta-coordination of this $UO_2F_4(H_2O)^{2-}$ dianion were confirmed by X-ray crystallography[19] and EXAFS in aqueous solution.[8b] The current work provides the first experimental evidence that $UO_2F_4^{2-}$ prefers tetra-coordination in the gas phase. The large negative charges on the F^- ligands due to the strong intramolecular Coulomb repulsion in the dianion account for the different coordination number between the gas phase and the condensed phase.

5.3. $UO_2F_4(CH_3CN)_n^{2-}$ ($n = 1, 2$)

The PES spectra of $UO_2F_4(CH_3CN)_n^{2-}$ ($n = 1, 2$) (Fig. 3) are similar to those of the corresponding hydrated complexes shown in Fig. 2, suggesting that the CH_3CN molecules interact with the $UO_2F_4^{2-}$ dianion in the outer sphere. We observed that the stabilization of CH_3CN to the electron binding energies is about 0.6 eV per solvent molecule relative to the VDE of $UO_2F_4^{2-}$ (Table 2). This observation indicates that the CH_3CN molecules interact more strongly with the $UO_2F_4^{2-}$ complex than water molecules. Our calculations show that each CH_3CN molecule can form three H-bonds from its CH_3 end to two F ligands on the equator and one axial O atom, forming a highly stable first solvation shell for $n = 2$. These solvation structures are consistent with two of our experimental observations. First, similar to the hydrated systems we have not observed $UO_2F_4^{2-}$ solvated by three CH_3CN molecules because the third molecule is expected to be more weakly bonded. Second, the additional H-bond with the axial O atom provides extra stabilization to the $UO_2F_4^{2-}$ dianion relative to H_2O, which only interacts with the equatorial F ligands. The simulated PES spectra of $UO_2F_4(CH_3CN)_n^{2-}$ (Fig. 10) are also consistent with the experimental observation.

It is surprising to observe that the H atoms in CH_3CN can form strong H-bonds. Previously, we observed H-bonding between the terminal CH_3 group and the $-CO_2^-$ group in long chain $CH_3(CH_2)_nCO_2^-$ carboxylates.[68] This type of H-bond is facilitated by the negative charge and the high charge density in the anion center. The $UO_2F_4^{2-}$ complex possesses high charge density, which makes it possible to form strong H-bonds between the complex and CH_3CN, as shown in Fig. 9. The large dipole moments on H_2O or CH_3CN also favor the H-bonding structures observed. A recent DFT study suggests that CH_3CN can interact more strongly with UO_2^{2+} *via* the N end than H_2O and the uranyl dication can accommodate five equatorial H_2O or CH_3CN ligands in the gas phase.[27] Despite the stronger interaction between CH_3CN and UO_2^{2+}, the current work shows clearly that CH_3CN does not directly coordinate to the U atom in $UO_2F_4(CH_3CN)_n^{2-}$ ($n = 1, 2$) in the gas phase.

6. Conclusions

We report the first experimental observation of the doubly charged $UO_2F_4^{2-}$ anion in the gas phase and its solvation complexes by one and two water or acetonitrile molecules. Photoelectron spectroscopy and *ab initio* theoretical calculations are used to probe the stability of $UO_2F_4^{2-}$ and its solvation structures. The $UO_2F_4^{2-}$ dianion is observed to be highly electronically stable with an adiabatic electron binding energy of 1.10 eV and a repulsive Coulomb barrier of about 2.0 eV. The photoelectron spectra of the solvated species are similar to that of the bare $UO_2F_4^{2-}$ dianion. Each water molecule is observed to stabilize the electron binding energy of $UO_2F_4^{2-}$ by about 0.5 eV and each CH_3CN molecule by about 0.6 eV. Theoretical calculations show that the frontier orbitals of $UO_2F_4^{2-}$ are mainly of U–O bonding characters and a high density of F 2p orbital below the HOMO. The U–F bond lengths are shown to decrease by about 0.1 Å in the $UO_2F_4^-$ monoanion relative to those in the $UO_2F_4^{2-}$ dianion, consistent with the broad photoelectron band for the ground state transition. All the solvent molecules are

shown to coordinate in the outer sphere, interacting with the F or O atoms. We have found that each water molecule forms two H-bonds with two F atoms, while each CH_3CN molecule forms three H-bonds with two F atoms and one axial O atom. These complexes provide ideal benchmarking systems to investigate the solvation effects on $UO_2F_4^{2-}$ and its gas-phase properties. The current study also demonstrates that electrospray ionization in combination with photoelectron spectroscopy is a valuable technique to probe the intrinsic electronic properties of uranyl complexes and their interactions with different ligands and solvents.

Acknowledgements

This work was supported by the U.S. Department of Energy, Office of Basics Energy Sciences under Grant No. DE-FG02-11ER16261. P. D. D. would like to thank the Nahigian Gift to the Department of Chemistry at Brown University for partial support of this work. The theoretical work was supported by NKBRSF (2011CB932400) and NSFC (20933003, 11079006, 91026003) of China. The calculations were performed using the DeepComp 7000 computer at the Supercomputer Center of the Computer Network Information Center, Chinese Academy of Sciences and the Shanghai Supercomputing Center.

References

1 L. R. Morss, N. M. Edelstein and J. Fuger, *The Chemistry of the Actinide and Transactinide Elements.* Springer, Dordrecht, Netherlands, 2006, vol. 1.
2 S. P. Mcglynn and J. K. Smith, *J. Mol. Spectrosc.*, 1961, **6**, 164.
3 M. Pepper and B. E. Bursten, *Chem. Rev.*, 1991, **91**, 719.
4 R. G. Denning, *Struct. Bonding*, 1992, **79**, 215.
5 R. G. Denning, *J. Phys. Chem. A*, 2007, **111**, 4125.
6 J. Su, K. Zhang, W. H. E. Schwarz and J. Li, *Inorg. Chem.*, 2011, **50**, 2082.
7 M. V. Ryzhkov and V. A. Gubanov, *J. Radioanal. Nucl. Chem.*, 1990, **143**, 85.
8 (*a*) M. Straka, K. G. Dyall and P. Pyykkö, *Theor. Chem. Acc.*, 2001, **106**, 393; (*b*) V. Vallet, U. Wahlgren, B. Schimmelpfennig, H. Moll, Z. Szabo and I. Grenthe, *Inorg. Chem.*, 2001, **40**, 3516.
9 G. S. Groenewold, M. J. van Stipdonk, J. Oomens, W. A. de Jong, G. L. Gresham and M. E. McIlwain, *Int. J. Mass Spectrom.*, 2010, **297**, 67.
10 C. Gaillard, A. Chaumont, I. Billard, C. Hennig, A. Ouadi and G. Wipff, *Inorg. Chem.*, 2007, **46**, 4815.
11 M. Harada, Y. Fujii, S. Sakamaki and H. Tomiyasu, *Bull. Chem. Soc. Jpn.*, 1992, **65**, 3022.
12 W. Aas, Z. Szabo and I. Grenthe, *J. Chem. Soc., Dalton Trans.*, 1999, 1311.
13 V. Vallet, U. Wahlgren, Z. Szabo and I. Grenthe, *Inorg. Chem.*, 2002, **41**, 5626.
14 T. Toraishi, T. Privalov, B. Schimmelpfennig, U. Wahlgren and I. Grenthe, *J. Phys. Chem. A*, 2003, **107**, 9456.
15 V. Vallet, H. Moll, U. Wahlgren, Z. Szabo and I. Grenthe, *Inorg. Chem.*, 2003, **42**, 1982.
16 Z. Fazekas, T. Yamamura and H. Tomiyasu, *J. Alloys Compd.*, 1998, **271**, 756.
17 L. F. Rao and G. X. Tian, *Inorg. Chem.*, 2009, **48**, 6748.
18 M. C. Chakravorti and N. Bandyopadhyay, *J. Inorg. Nucl. Chem.*, 1971, **33**, 2565.
19 T. C. W. Mak and W. H. Yip, *Inorg. Chim. Acta*, 1985, **109**, 131.
20 M. Bühl, *Can. J. Chem.*, 2009, **87**, 818.
21 G. Schreckenbach, P. J. Hay and R. L. Martin, *J. Comput. Chem.*, 1999, **20**, 70.
22 I. Infante and L. Visscher, *J. Comput. Chem.*, 2003, **25**, 386.
23 M. Garcia-Hernandez, C. Willnauer, S. Kruger, L. V. Moskaleva and N. Rösch, *Inorg. Chem.*, 2006, **45**, 1356.
24 M. Bühl, G. Schreckenbach, N. Sieffert and G. Wipff, *Inorg. Chem.*, 2009, **48**, 9977.
25 M. Bühl, N. Sieffert and G. Wipff, *Chem. Phys. Lett.*, 2009, **467**, 287.
26 F. Ruiperez and U. Wahlgren, *J. Phys. Chem. A*, 2010, **114**, 3615.
27 M. Bühl, N. Sieffert, A. Chaumont and G. Wipff, *Inorg. Chem.*, 2011, **50**, 299.
28 G. Schreckenbach, S. O. Odoh, S. M. Walker, M. Meier and J. Stetefeld, *Inorg. Chem.*, 2011, **50**, 3141.
29 C. Moulin, N. Charron, G. Plancque and H. Virelizier, *Appl. Spectrosc.*, 2000, **54**, 843.
30 C. Moulin, B. Amekraz, D. Doizi, G. Plancque and V. Steiner, *J. Inorg. Biochem.*, 2001, **86**, 347.
31 M. J. van Stipdonk, V. Anbalagan, W. Chien, G. Gresham, G. S. Groenewold and D. Hanna, *J. Am. Soc. Mass Spectrom.*, 2003, **14**, 1205.
32 S. P. Pasilis and J. E. Pemberton, *Inorg. Chem.*, 2003, **42**, 6793.
33 W. Chien, V. Anbalagan, M. Zandler, M. J. van Stipdonk, D. Hanna, G. Gresham and G. S. Groenewold, *J. Am. Soc. Mass Spectrom.*, 2004, **15**, 777.
34 V. Anbalagan, W. Chien, G. L. Gresham, G. S. Groenewold and M. J. van Stipdonk, *Rapid Commun. Mass Spectrom.*, 2004, **18**, 3028.
35 M. J. van Stipdonk, W. Chien, V. Anbalagan, K. Bulleigh, D. Hanna and G. S. Groenewold, *J. Phys. Chem. A*, 2004, **108**, 10448.
36 M. J. van Stipdonk, W. Chien, K. Bulleigh, Q. Wu and G. S. Groenewold, *J. Phys. Chem. A*, 2006, **110**, 959.
37 A. Somogyi, S. P. Pasilis and J. E. Pemberton, *Int. J. Mass Spectrom.*, 2007, **265**, 281.
38 G. S. Groenewold, A. K. Gianotto, K. C. Cossel, M. J. van Stipdonk, D. T. Moore, N. Polfer, J. Oomens, W. A. de Jong and L. Visscher, *J. Am. Chem. Soc.*, 2006, **128**, 4802.
39 G. S. Groenewold, M. J. van Stipdonk, W. A. de Jong, J. Oomens, G. L. Gresham, M. E. Mcllwain, D. Gao, B. Siboulet, L. Visscher, M. Kullman and N. Polfer, *Chem. Phys. Chem.*, 2008, **9**, 1278.
40 G. S. Groenewold, J. Oomens, W. A. de Jong, G. L. Gresham, M. E. McIlwain and M. J. van Stipdonk, *Phys. Chem. Chem. Phys.*, 2008, **10**, 1192.
41 G. S. Groenewold, W. A. de Jong, J. Oomens and M. J. Van Stipdonk, *J. Am. Soc. Mass Spectrom.*, 2010, **21**, 719.
42 L. S. Wang, C. F. Ding, X. B. Wang and S. E. Barlow, *Rev. Sci. Instrum.*, 1999, **70**, 1957.
43 (*a*) L. S. Wang, X. B. Wang and C. F. Ding, *Phys. Rev. Lett.*, 1998, **81**, 3351; (*b*) X. B. Wang and L. S. Wang, *Nature*, 1999, **400**, 245; (*c*) L. S. Wang and X. B. Wang, *J. Phys. Chem. A*, 2000, **104**, 1978; (*d*) X. B. Wang and L. S. Wang, *Annu. Rev. Phys. Chem.*, 2009, **60**, 105.
44 (*a*) C. F. Ding, X. B. Wang and L. S. Wang, *J. Phys. Chem. A*, 1998, **102**, 8633; (*b*) X. B. Wang, J. B. Nicholas and L. S. Wang, *J. Chem. Phys.*, 2000, **113**, 10837; (*c*) X. B. Wang, X. Yang, J. B. Nicholas and L. S. Wang, *Science*, 2001, **294**, 1322; (*d*) X. B. Wang, X. Yang and L. S. Wang, *Int. Rev. Phys. Chem.*, 2002, **21**, 473.
45 J. P. Perdew, K. Burke and M. Ernzerhof, *Phys. Rev. Lett.*, 1996, **77**, 3865.
46 ADF 2010.01, http://www.scm.com.
47 C. F. Guerra, J. G. Snijders, G. te Velde and E. J. Baerends, *Theor. Chem. Acc.*, 1998, **99**, 391.
48 G. T. Velde, F. M. Bickelhaupt, E. J. Baerends, C. F. Guerra, S. J. A. van Gisbergen, J. G. Snijders and T. Ziegler, *J. Comput. Chem.*, 2001, **22**, 931.
49 E. van Lenthe and E. J. Baerends, *J. Comput. Chem.*, 2003, **24**, 1142.
50 E. van Lenthe, E. J. Baerends and J. G. Snijders, *J. Chem. Phys.*, 1993, **99**, 4597.
51 H. J. Werner, *MOLPRO*, version 2008.1, http://www.molpro.net.
52 X. B. Wang, Y. L. Wang, J. Yang, X. P. Xing, J. Li and L. S. Wang, *J. Am. Chem. Soc.*, 2009, **131**, 16368.
53 Y. L. Wang, H. J. Zhai, L. Xu, J. Li and L. S. Wang, *J. Phys. Chem. A*, 2010, **114**, 1247.
54 Y. L. Wang, X. B. Wang, X. P. Xing, F. Wei, J. Li and L. S. Wang, *J. Phys. Chem. A*, 2010, **114**, 11244.
55 K. Kowalski and P. Piecuch, *J. Chem. Phys.*, 2004, **120**, 1715.
56 M. Valiev, E. J. Bylaska, N. Govind, K. Kowalski, T. P. Straatsma, H. J. J. Van Dam, D. Wang, J. Nieplocha, E. Apra, T. L. Windus and W. de Jong, *Comput. Phys. Commun.*, 2010, **181**, 1477.
57 http://www.theochem.uni-stuttgart.de/pseudopotential.

58 A. Nicklass, M. Dolg, H. Stoll and H. Preuss, *J. Chem. Phys.*, 1995, **102**, 8942.
59 R. A. Kendall, T. H. Dunning and R. J. Harrison, *J. Chem. Phys.*, 1992, **96**, 6796.
60 (*a*) X. B. Wang, C. F. Ding and L. S. Wang, *Chem. Phys. Lett.*, 1999, **307**, 391; (*b*) X. B. Wang and L. S. Wang, *Phys. Rev. Lett.*, 1999, **83**, 3402.
61 The $UO_2F_3^-$ anion was produced directly from the ESI source. However, we were unable to detect the photoelectron signals even at 157 nm due to its high electron binding energy. Preliminary theoretical calculation suggested the electron binding energy of $UO_2F_3^-$ is >7 eV.
62 X. B. Wang, Y. L. Wang, H. K. Woo, J. Li, G. S. Wu and L. S. Wang, *Chem. Phys.*, 2006, **329**, 230.
63 E. van Lenthe, J. G. Snijders and E. J. Baerends, *J. Chem. Phys.*, 1996, **105**, 6505.
64 (*a*) D. A. Case and C. Y. Yang, *J. Chem. Phys.*, 1980, **72**, 3443; (*b*) H. Xiao, H. S. Hu, W. H. E. Schwarz and J. Li, *J. Phys. Chem. A*, 2010, **114**, 8837.
65 F. Wei, G. S. Wu, W. H. E. Schwarz and J. Li, *J. Chem. Theory Comput.*, 2011, **7**, 3223.
66 J. Su, Y. L. Wang, F. Wei, W. H. E. Schwarz and J. Li, *J. Chem. Theory Comput.*, 2011, **7**, 3293.
67 M. Zhou, L. Andrews, J. Li and B. E. Bursten, *J. Am. Chem. Soc.*, 1999, **121**, 9712.
68 X. B. Wang, H. K. Woo, B. Kiran and L. S. Wang, *Angew. Chem., Int. Ed.*, 2005, **44**, 4968.

